sciendo

POLISH MARITIME RESEARCH 2 (106) 2020 Vol. 27; pp. 96-106
10.2478/pomr-2020-0031

INFLUENCE OF SURFACE TEXTURE PARAMETERS ON FRICTION CHARACTERISTICS UNDER STARVED LUBRICATION

Shen Wu
Pan Zhang
Haijun Wei
Lei Chen
Shanghai Maritime University, China

ABSTRACT

A cylinder liner and piston ring running under starved lubrication near the top dead centre (TDC) and bottom dead centre (BDC) cause abnormal friction and wear during operation of a marine diesel engine. The method of laser texturing is proposed to improve the surface friction property under this condition. Spherical crown pits with different parameters were formed on the surface of samples by femtosecond laser processing. The BDC and TDC conditions of oil starvation were simulated in a reciprocating friction and wear experiment, and a numerical model of surface texture lubrication based on the Reynolds equation was established. The influence of the distribution density, diameter, and depth parameters of the texture on the surface properties was studied. In the BDC condition, compared with the untextured surface, the average coefficient of friction (COF) can be reduced by up to 24% and the average friction force can be reduced by up to 18%. In the TDC condition, the COF can be reduced by up to 19%, and the average friction force can be reduced by up to 18%. Therefore, the textures with various parameters should be arranged in different positions on the cylinder liner; more attention should be paid to the optimisation of diameter in the texture of the cylinder liner near the BDC, whereas more attention should be paid to the optimisation of distribution density in the texture of the cylinder liner near the TDC

Keywords: Marine diesel engine; Cylinder liner and piston ring; Friction reduction; Starved lubrication; Laser texturing

INTRODUCTION

The internal combustion engine is the main power equipment widely used in ships. The piston runs at a low speed near the top dead centre (TDC) and bottom dead centre (BDC), especially in high-temperature and high-pressure conditions near the TDC. During the operation of low-speed two-stroke marine diesel engines, the local maximum temperature in the cylinder can reach up to 2200°C and the temperature of the exhaust gas can reach up to 300°C. Under the combined effects of combustion, friction, and cooling, the working temperature of the cylinder liner-piston ring friction pair can reach up to 200°C [1]. The friction pair of the cylinder liner and the piston ring working in the state of mixed or boundary lubrication leads to serious problems of abnormal friction and wear [2]. Therefore, it is very important to improve the mechanical state of the friction pair, which has great potential to provide energy savings and emissions reductions.

Texturing is a modern surface treatment technology. The friction properties can be effectively improved by processing regular pits or grooves. At present, related researches mainly focus on the lubrication and friction mechanism of surface texture [3–6]. Etsion et al. [7] believed that each pit plays the role of a hydrodynamic bearing under full and mixed lubrication so as to improve the bearing capacity of the oil film. Arslan et al. [8] studied the tribological properties of different sizes pits and found that performance enhancement could be obtained at an optimum pit diameter and depth. Wang et al. [9, 10] studied the bearing capacity of silicon carbide ceramics with surface texture under water lubrication and found that

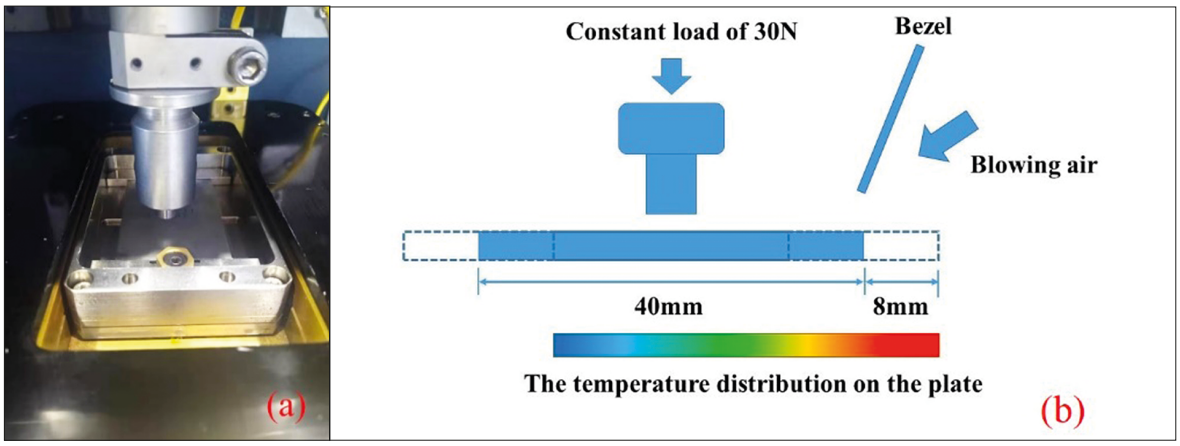

Fig. 1. The tribometer (a) and air blowing on the surface of samples (b)

different lubrication conditions required surface textures with different geometric features to achieve good results. Ronen et al. [11] established a mathematical model for reciprocating motion between the piston ring and the cylinder liner with surface texture and studied the influence of pit depth, diameter, and area ratio on friction performance. The results showed that the ratio of depth to diameter has a great influence on the friction performance.

During the working process of the internal combustion engine, the piston speed at the BDC is almost zero. The running state is worse at the position of the TDC (the piston speed is almost zero) and under conditions of high temperature and pressure. The oil film is extremely thin, and under mixed or boundary lubrication, more oil film bursts and changes to a dry friction condition [12]. The lubrication and friction state of a textured surface is influenced by various effects, which means that the mechanism is very complex and difficult to study [13–16]. At present, experimental research on the friction property of surface texture is mainly focused on the full oil condition, which is generally only applicable to simulation of the position near the middle of the piston stroke [17–20]. However, there are few researches on the friction characteristics of textured surfaces under the mixed or boundary lubrication state of the BDC and TDC. In this paper, the effects of different texture parameters on the friction properties of textured surfaces were studied by simulating high-temperature, high-pressure, and low-speed conditions in reciprocating experiments. From the results, the order of priority of parameters used to design texture under different working conditions is obtained, providing a reference for further optimisation of textured surfaces.

EXPERIMENTAL DESIGN

EXPERIMENTAL PLATFORM

The reciprocating test was carried out on a friction and wear test machine (UMT-TriboLab), and the structure of the experimental platform is shown in Fig. 1(a). The crank mechanism converts the rotary motion of the slider into a reciprocating motion, allowing simultaneous control of the reciprocating speed and the load applied on the contact surface of the sample. During the experiment, the real-time friction force and the load on the surface of the friction pair were measured by a high-performance sensor (DFH-5G, range: 0.5–50 N, resolution: 2.5 mN).

SAMPLE PREPARATION

In order to simulate the running conditions of the cylinder liner and the piston ring accurately, the samples were made of nodular cast iron. The material components are shown in Table 1. All samples had a hardness of 170 HBS. The samples included upper pin samples and lower plate samples. The upper samples were pins with a diameter of 6 mm and a length of 20 mm and were fixed. The size of the plate samples was 34 mm * 40 mm, and the samples were fixed on the slider for reciprocating motion.

Table 1. Composition of experimental nodular cast iron

C	Si	Mn	P	S	Mg
3.62%	2.43%	0.182%	0.047%	0.004%	0.057%

In order to explore the influence of texture parameters on the friction property of the surface, the femtosecond laser processing method was used to obtain high-precision spherical crown pits with diameters of 100, 150, and 200 μm, depths of 20, 30, and 40 μm and distribution densities of 3, 5, and 8% on the surface of the samples, respectively. The surface distribution density was defined as the ratio of the area of the pit to the unit area in which it was located, as shown in Fig. 2 and Eq. 1.

$$S_p = \frac{\pi d^2}{4L^2} \tag{1}$$

where S_p is the distribution density, d is the diameter of the texture pit, and L is the side length of the unit.

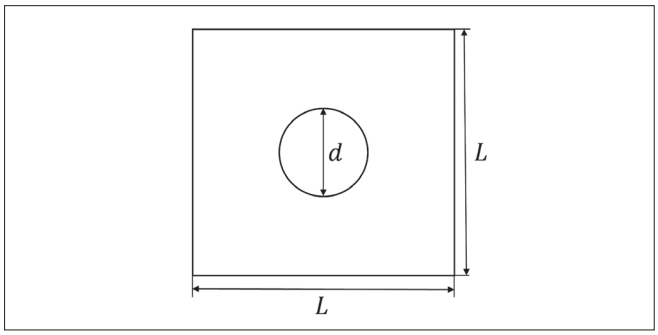

Fig. 2. The geometric shape of texture pits

The morphology of the textured surface is shown in Fig. 3. The initial surface roughness of the samples was reduced to Ra 0.2 μm by polishing.

EXPERIMENTAL DETAILS

The friction and wear test machine was used to simulate the reciprocating movement of the cylinder liner and piston ring. The reciprocating stroke was set to 16 mm (one work cycle includes two strokes), and the reciprocating frequency was set to 6, 8, and 10 Hz, corresponding to average speeds of 0.192, 0.256, and 0.32 m/s, respectively. A constant load of 30 N (corresponding to a contact pressure of 1.06 MPa) was chosen. Mobilgard 412 marine lubricating oil was selected to maintain the state of oil starvation. The kinematic viscosity of this brand of oil was 120 mm^2/s at 40°C and 12 mm^2/s at 100°C.

In order to simulate the condition of oil starvation near the BDC, only a thin oil film was retained on the surface of the friction pair in the experiment. Before each experiment, the residual oil on the surface was cleaned with gasoline, 0.5 ml of lubricating oil was added, and the lubricating oil was spread out gently with rubber pieces. After scraping the oil several times, the oil film on the surface would be extremely thin. In order to simulate the high-temperature and high-pressure conditions near the TDC, the oil was scraped before the movement, and high-temperature compressed air was blown at the end of the reciprocating stroke. The pressure of the compressed air outlet was set to 0.5 MPa. The compressed air was constant and the blow area was limited by a bezel, as shown in Fig. 1(b). The temperature distribution on the plates was monitored by laser thermometer. Air blows were began when the pin samples reached the end of the stroke. Electric wire was arranged at the outlet of the compressed air to maintain the high-temperature blows of air. Under the purging by high-temperature compressed air, the oil film became much thinner than before and reached the mixed lubrication state.

Before each experiment, the pin-plate friction pairs were run for 20 minutes under the condition of 30 N and 8 Hz. The experiment was started after the friction coefficient had become stable. The low-speed and starved oil condition of the BDC was simulated in the front section of the experiment, and the experiment was conducted for 4 minutes after the oil had been scraped. Starting from the fifth minute, the condition of high temperature and high pressure of the TDC was simulated. The compressed air switch was turned on and the samples were purged intermittently with the reciprocating movement. After that, the compressed air switch was turned off and the experiment finished. During the experiment, the values of the friction force on the surface and the normal load force were measured. During the single experiment, the average value in the process was taken as the result.

LUBRICATION SIMULATION MODEL

Considering the single pit and the two-dimensional situation, the physical model of the spherical crown surface texture was established, as shown in Fig. 4. Among them, the upper surface remains relatively stationary, the sliding speed of the lower

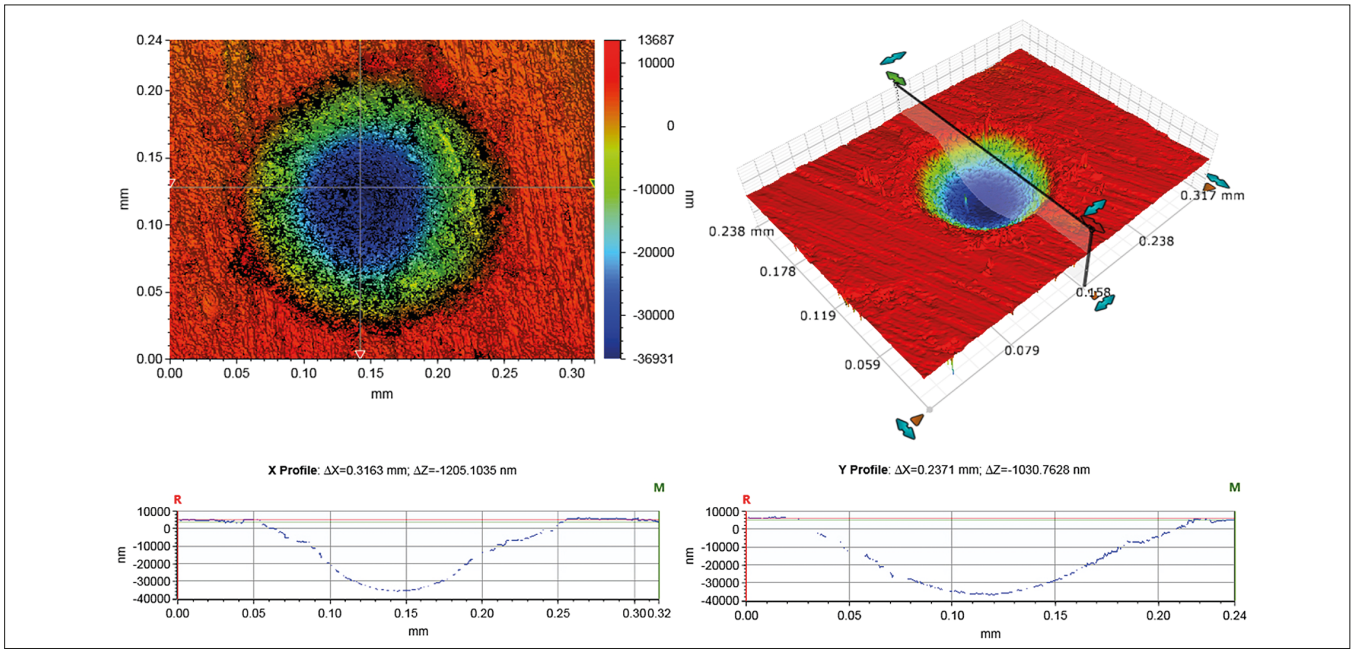

Fig. 3. The morphology of the textured surface

surface is , the initial distance between the two planes of the friction pair is , and the maximum pit depth is .

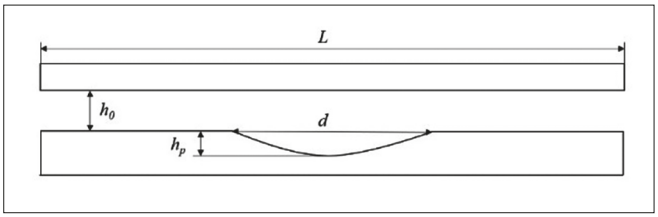

Fig. 4. The physical model of the spherical crown surface pit

Based on the Reynolds equation, a numerical model for the lubrication of textured surfaces was established, as shown in Eqs. (2–4). In order to simplify and facilitate the analysis and calculation, the following assumptions were made: (1) the effect of bulk force could be ignored; (2) lubricating oil is an incompressible fluid with a constant viscosity; (3) steady state conditions were considered; (4) there was a symmetrical distribution along the z-plane, considering only a two-dimensional surface texture [21].

$$\frac{\partial}{\partial x_1}\left(h^3\frac{\partial p}{\partial x_1}\right)+\frac{\partial}{\partial x_2}\left(h^3\frac{\partial p}{\partial x_2}\right)=6u\eta\frac{\partial h}{\partial x_1} \tag{2}$$

where x_1 and x_2 are two coordinate directions; is the thickness of the lubricant film; p is the pressure of the oil film; u is the relative sliding speed between the surfaces of the two friction pairs; and η is the viscosity of the lubricant in the region of the texture unit.

The oil film thickness can be expressed by the equation:

$$h(x_1, x_2)=\begin{cases}h_0+\Delta h & \in\Omega_+\\ h_0 & (x_1, x_2)\in\Omega_0\end{cases} \tag{3}$$

$$\Delta h=\frac{h_p}{r}\sqrt{r^2-(x_1, x_{1c})^2-(x_2, x_{2c})^2},\ r=d/2 \tag{4}$$

where x_{1c} and x_{2c} are the distances from the node to the centre point of the texture pit in the directions of x_1 and x_2. The upper and lower borders adopt symmetrical conditions; that is, the pressure value of the grid nodes on the border is equal to the pressure of the adjacent grid nodes in the calculation area. The pressures at the left and right borders are taken as atmospheric pressure, and the Reynolds space is introduced into the calculation. The boundary conditions are modified to correct the pressure [22].

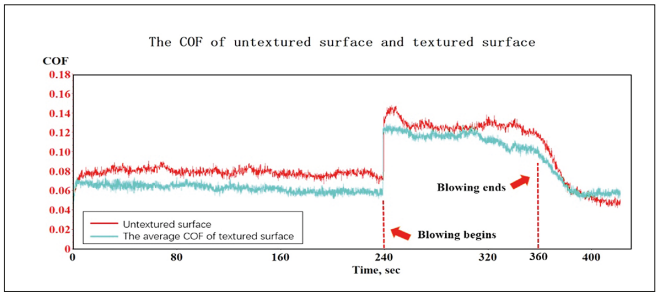

Fig. 5. Comparison of COF between untextured and textured surfaces

EXPERIMENTAL RESULTS AND DISCUSSION

COMPLETE EXPERIMENTAL RESULTS AND ANALYSIS

Figure 5 shows the variation trend of the average coefficient of friction (COF) under the conditions of the BDC and TDC. As can be seen in the figure, during the first four minutes of the experiment, the COF was relatively stable, within the range of 0.07–0.10. According to Stribeck theory, under this working condition, the friction pair was in the state of mixed lubrication and there was viscous shear force inside the lubricating oil, as well as the local contact of the micro-convex body on the metal surface. Starting from the fifth minute, under the blowing of high-temperature compressed air, the oil film on the surface decreased sharply, the distance between the surfaces in relative movement decreased, the number of contact micro-convex bodies on the metal surface increased, and the friction pair was in the mixed or even boundary lubrication state [23]. At this time, the COF increased sharply, reaching about 0.12–0.14. After the compressed air switch was turned off, the oil film on the surface was no longer blown and began to flow back slowly. During this process, the amount of lubricating oil increased slowly, the thickness of the oil film gradually increased, and the distance between friction surfaces increased, so the number of micro-convex contacts decreased and the COF slowly dropped.

Figure 6 shows a comparison of the average oil film pressure distribution on the untextured surface and the textured surfaces calculated by the simulation model. The dimensionless parameters were used on the axes. The pit

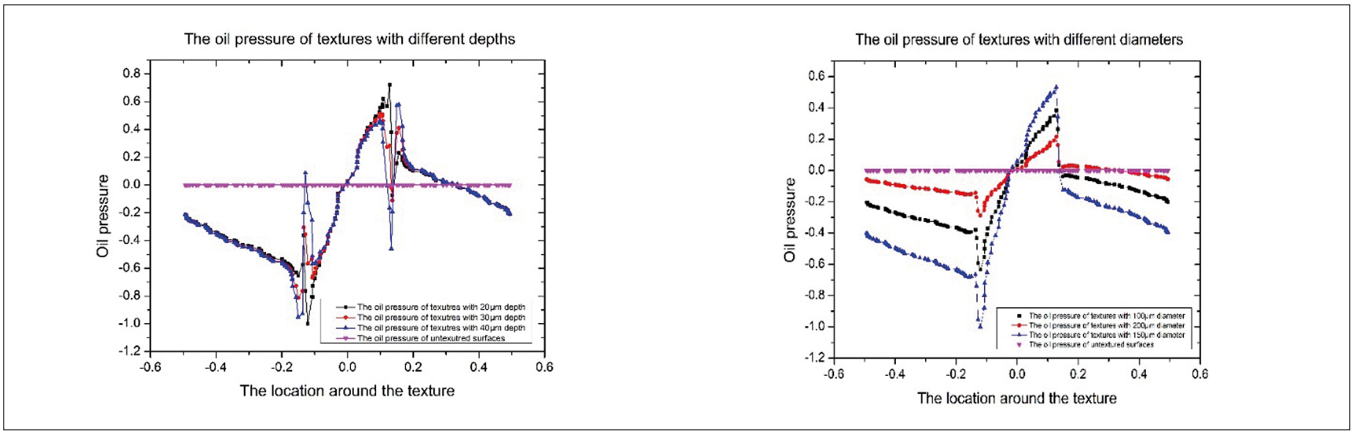

Fig. 6. The pressure distribution of pits with different depths (a) and the pressure distribution of textures with different diameters (b) in a texture pit

diameter was normalized to –0.5 to 0.5. The x axis represents the geometric diameter of a single pit, and the y axis represents the average pressure generated. It can be found that different asymmetric oil-film support pressures can be generated near the pit texture with different parameters, showing different friction-reduction effects. But the trends of pressure distribution in Fig. 6 are different. The pressures generated in Fig. 6(a) appeared in the ranges of –0.2 to –0.1 and 0.1 to 0.2, and the pressures generated in Fig. 6(b) appeared in the ranges of –0.5 to 0.5, indicating that the distributions of oil film pressure were affected by different factors in Fig. 6(a) and (b). The effects of depth and diameter on the oil film support pressures were different.

Comparing the average COF curves of the textured and untextured surfaces, it can be found that the COF of the textured surface was lower than that of the untextured surface in the whole process, which indicated that the surface texture plays a certain role in friction reduction. In the process of relative motion, the oil inside the surface texture formed an asymmetric oil-film pressure, which could play the role of a micro-bearing, increased the distance between the surfaces, and reduced the contact between micro-convex bodies. At the same time, under the action of high-temperature and high-pressure air blowing, the surface texture played a role in oil storage [24] allowing more lubricating oil to be retained. After the compressed air switch was turned off, the oil storage function of the texture on the surface was further revealed. The regular textured surface can accelerate the returning flow of the oil, which makes the thickness of the oil film between the friction pair increase faster and reduces the time during which the friction pair are in bad working conditions.

EXPERIMENTAL RESULTS AND ANALYSIS OF THE WORKING CONDITION OF BDC

Figures 7, 8, and 9 show the change of COF and friction force with the various texture distribution densities (diameter of 150 μm, depth of 30 μm). In the experiment with densities of 3, 5, and 8%, the COF and friction force first decreased and then increased with the increase of texture density. The density of 5% gave the smallest COF and friction force, which were up to 11 and 7% lower, respectively, compared with the untextured surface, providing the optimal anti-friction property in the experiment. Figures 10, 11, and 12,

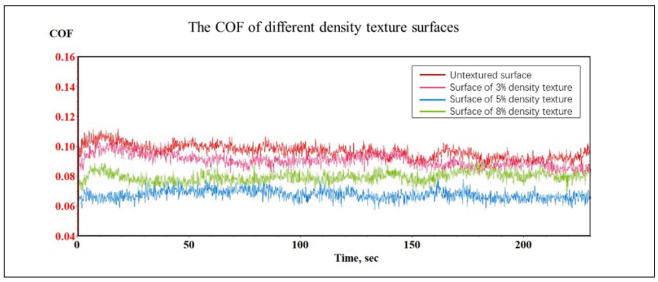

Fig. 7. The COF of surfaces with texture densities of 3, 5, and 8%

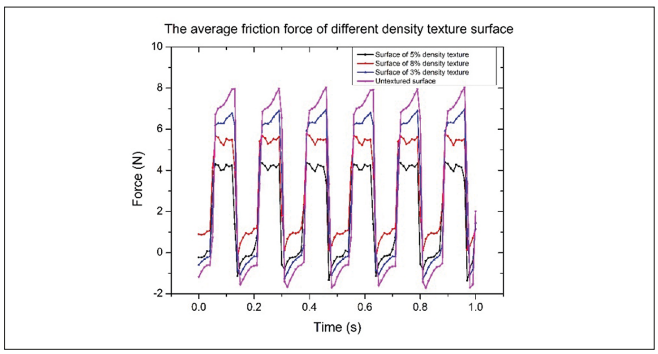

Fig. 8. The friction force of surfaces with texture densities of 3, 5, and 8%

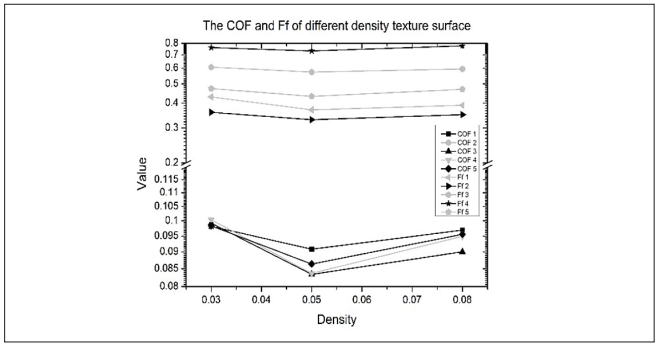

Fig. 9. The trend of friction characteristics of surfaces with texture densities of 3, 5, and 8%

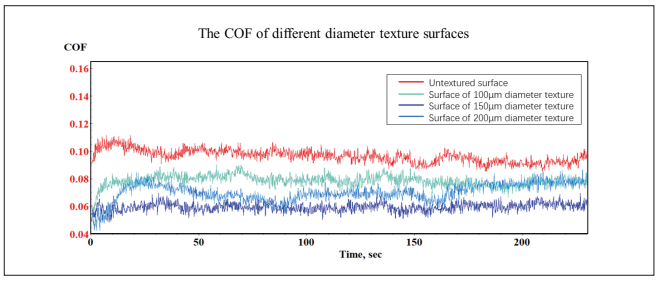

Fig. 10. The COF of surfaces with pit diameters of 100, 150, and 200 μm

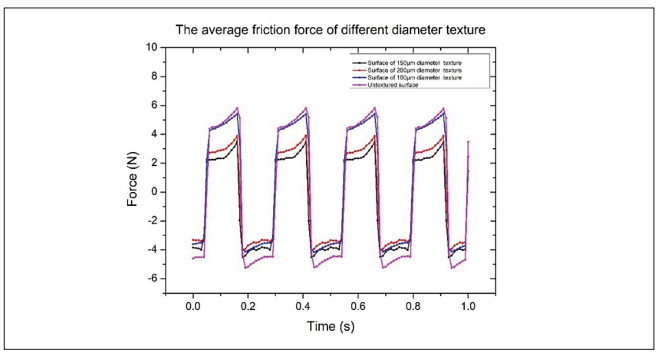

Fig. 11. The friction force of surfaces with pit diameters of 100, 150, and 200 μm

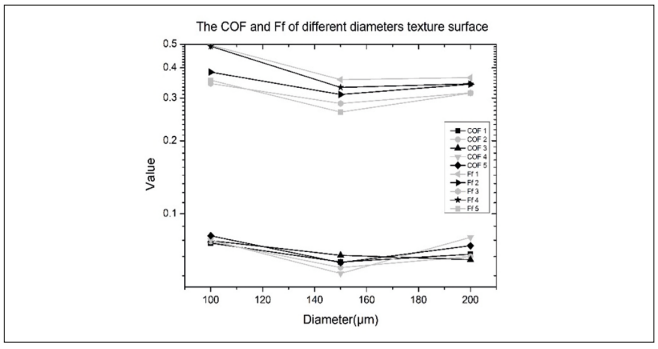

Fig. 12. The trend of friction characteristics of surfaces with pit diameters of 100, 150, and 200 μm

respectively, show the change of COF and friction force with various pits diameters (density of 5%, depth of 20 μm). Among the diameter parameters of 100, 150, and 200 μm, the COF and friction force first decreased and then increased with the increase of pits diameter. The 150-μm diameter gave the lowest COF and friction force, which were 24% and 18% lower, respectively, compared with the untextured surface.

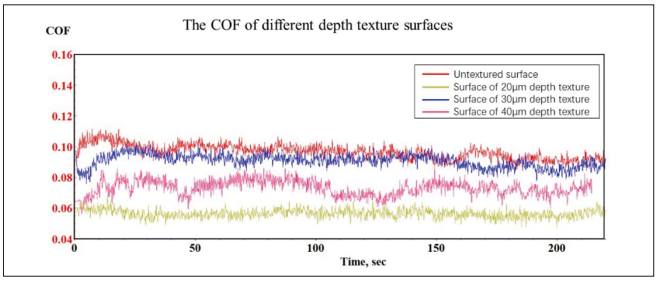

Fig. 13. The COF of surfaces with pits depths of 20, 30, and 40 μm

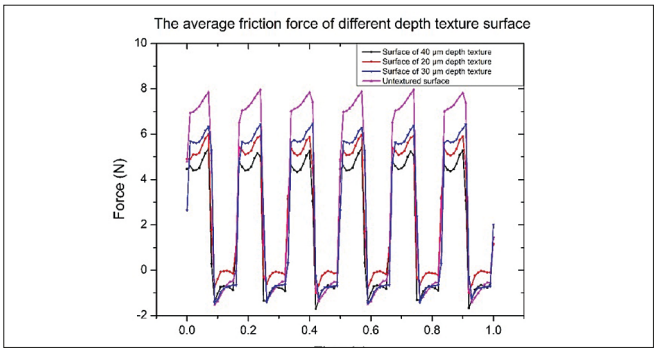

Fig. 14. The friction force of surfaces with pits depths of 20, 30, and 40 μm

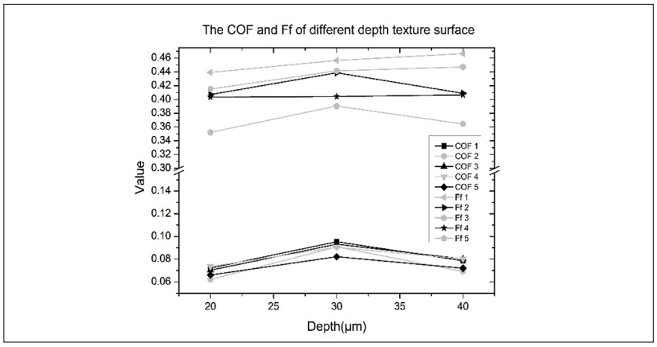

Fig. 15. The trend of friction characteristics of surfaces with pits depths of 20, 30, and 40 μm

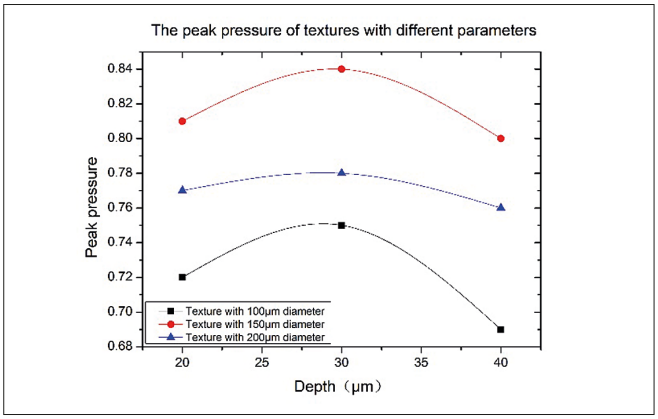

Fig. 16. The peak pressures of pits with different parameters

Figures 13, 14, and 15, respectively, show the change of COF and friction force with pit depth (density of 5%, diameter of 100 μm). Among the three sample groups with depth parameters of 20, 30, and 40 μm, the COF and friction force show a trend of first increasing and then decreasing with increases in pit depth. The 30-μm depth gave the maximum COF and friction force, and the 20-μm depth gave the minimum COF and friction force, which were 17% and 9% lower, respectively, compared with the untextured surface. The support force of the surface oil film decreased significantly and then increased slightly with increases of the pits diameter.

Figure 16 shows the oil film peak pressures of pits with different parameters. Dimensionless parameters were used on the axes. The x axis represents the diameter of pits, and the y axis represents the peak pressure of the oil film. The support force of the surface oil film increased with increases in the pits diameter but decreased significantly and then increased slightly with increases of the pits depth. The numerical calculation results show the same trend as in the literature [25] but are slightly different from the experimental results because the numerical model does not take into account the influence of complex factors such as the surface roughness of the sample on the state of the oil film during the experiment.

In the simulated BDC starved oil condition, thin oil film can be formed on the surface of the friction pair to support the surfaces in relative movement, and there will be a small amount of metal micro-convex contact. Compared with the untextured surface, the textured surface has an obvious anti-friction effect. The asymmetric oil film pressure formed inside the surface texture can provide additional support force for the surface of the friction pair, which is beneficial for reducing wear. At the same time, the actual contact area of the friction surface can be reduced in the process of texture processing, which reduces the contact of the micro-convex body in the process of motion but also increases the macroscopic surface roughness [26].

During the process of a density increase, the number of textures per unit area increases, and the supporting force provided by the oil film also increases, so the contact of the surface micro-convex body is reduced, the surface friction property is improved, and the COF and friction force are reduced accordingly. When the density increased by more than 5%, the friction caused by the increase of surface roughness far exceeded the anti-friction effect caused by the supporting force of the oil film, thus leading to increases of the COF and friction force. As the diameter of the pits increased from 100 to 150 μm, more oil could be held in the pits and more oil film support could be provided, thus reducing the COF and friction force. When the diameter increased to more than 150 μm, the lubricating oil in the pits was distributed more strongly by the friction surface, leading to chaos of the flowing state in the pits, which had a negative impact on the supporting force of the lubricating oil film and also increased the viscous force in the fluid, resulting in an increase of the COF and friction force. In the process of increasing the depth of the pit from 20 to 30

μm, although the oil quantity inside the pit increased, the flow distance between the surface and the bottom of the pits also increased. As a result, the supporting force of the oil film was greatly weakened, and the COF and friction force increased accordingly. When the depth continued to increase, the volume of oil held increased with a cubic trend. A large amount of oil can produce a strong oil-film supporting force, which can offset the negative effect caused by the flow distance. Therefore, the COF and friction force then decrease.

EXPERIMENTAL RESULTS AND ANALYSIS OF THE WORKING CONDITIONS OF THE TDC

As can be seen from Figs. 17–22, the variation trends of the COF and friction force with the distribution density and diameter were the same as those of the condition of the BDC, and the optimal anti-friction property was obtained under the parameters of 5% density and 150 μm diameter, respectively. The COF and friction force can be reduced by up to 19% and 18% at the density of 5% and by up to 10% and 4% at the diameter of 150 μm.

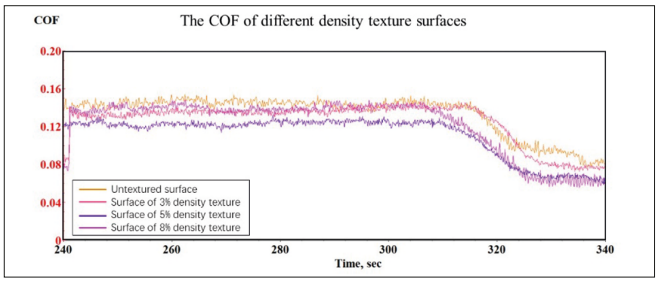

Fig. 17. The COF of surfaces with texture densities of 3, 5, and 8%

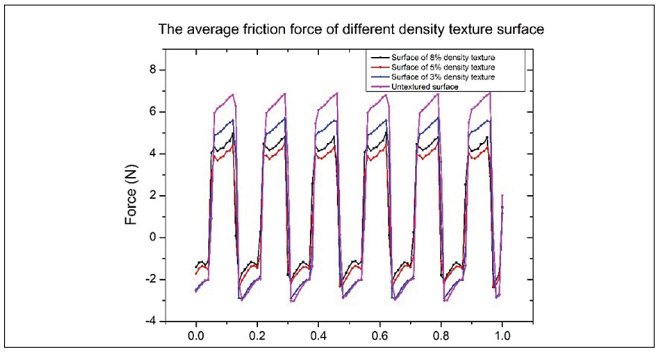

Fig. 18. The friction force of surfaces with texture densities of 3, 5, and 8%

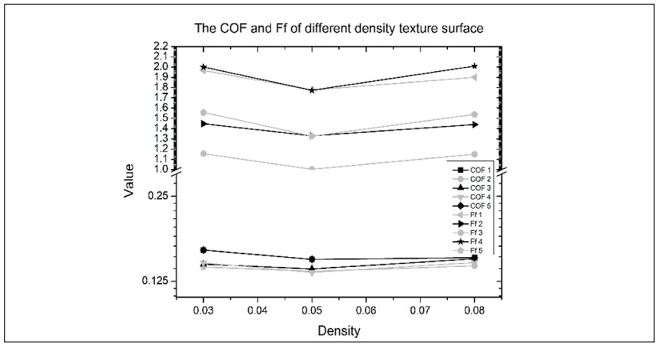

Fig. 19. The trend of friction characteristics of surfaces with texture densities of 3, 5, and 8%

In Figs. 23–25, the variation trends of the COF and friction force with pit depth are slightly different from those under the condition of the BDC. Although the COF and friction force first increased and then decreased, the optimal friction reduction property was obtained at 50 μm, which could reduce the COF and friction force by up to 13% and 12%. This is because when the depth of the pit reaches a certain value, a deep pit will be less affected by the blowing of high-temperature compressed air and can retain more lubricating oil after the blowing. At the same time, the oil at the bottom of the pit is less disturbed and the flow state is more stable, which can provide a larger oil-film supporting force. Therefore, the effect of the depth parameter on the reduction in surface friction is more obvious.

EXPERIMENTAL RESULTS AND ANALYSIS OF THE OPTIMAL COMBINATION OF PARAMETERS

The experimental results show that under the simulated conditions of the BDC, a distribution density of 5%, a diameter of 150 μm, and a depth of 20 μm are the parameters with the

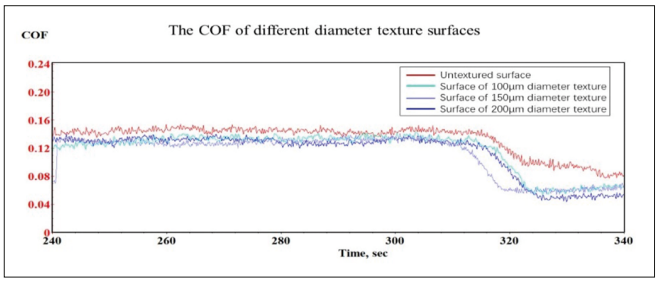

Fig. 20. The COF of surfaces with pits diameters of 100, 150, and 200 μm

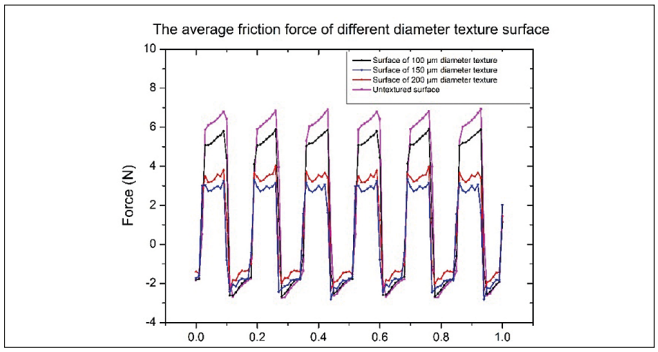

Fig. 21. The friction force of surfaces with pits diameters of 100, 150, and 200 μm

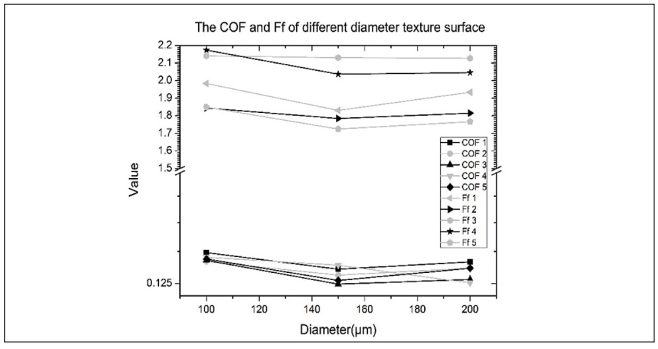

Fig. 22. The trend of friction characteristics of surfaces with pits diameters of 100, 150, and 200 μm

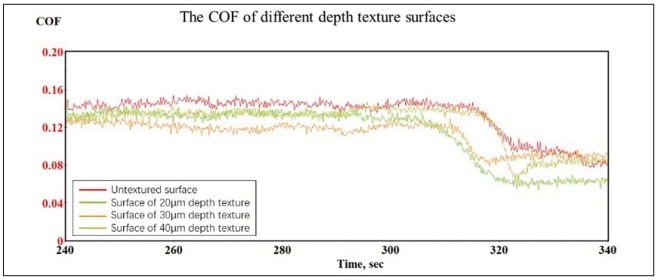

Fig. 23. The COF of surfaces with pits depths of 20, 30, and 40 μm

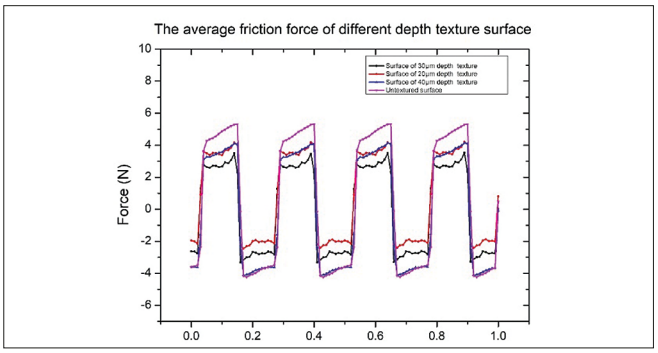

Fig. 24. The friction force of surfaces with pits depths of 20, 30, and 40 μm

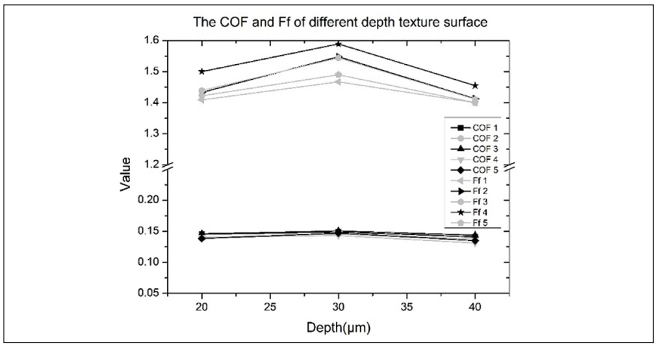

Fig. 25. The trend of friction characteristics of surfaces with pits depths of 20, 30, and 40 μm

best anti-friction property. Under the simulated condition of the TDC, a distribution density of 5%, a diameter of 150 μm, and a depth of 40 μm are the parameters with the best anti-friction property. Therefore, the pits with these parameter configurations was processed on the surface of the samples made of the same material by laser processing, and the friction and wear experiments were carried out under the same simulated conditions. However, on comparing the COF and friction force under the working conditions of two kinds of simulations, the surfaces having a combination of three optimal parameters did not achieve the best anti-friction effect, which may be the result of the coupling of different mechanisms.

In this paper, the effect of texture parameters on the anti-friction property under two kinds of working conditions was analysed, and the results are shown in Figs. 26–28. It can be seen that the diameter of the surface texture is the most important factor affecting the friction property under the condition of the simulated BDC. By changing the pits diameter in multiple experiments, the COF could be reduced by 24% on average and the friction force could be reduced by 18%. Secondly, the pits depth could reduce the COF by 17% on average and the friction force could be reduced by 9%. The distribution density had the least effect on the anti-friction performance, being able to reduce the COF and friction force by 11% and 7%, respectively. In the simulated TDC condition, the distribution density was the parameter that had the greatest influence on the anti-friction property of the texture. By changing the texture density in multiple experiments, the COF could be reduced by 19% on average and the friction could be reduced by 18%. The second was the depth, which could reduce the COF by 13% on average and could reduce the friction force by 12%. The diameter had the least influence on the anti-friction performance, and the COF and the friction force could be reduced by 10% and 4%, respectively.

In order to avoid a large amount of repetitive work, the priority parameters of texture design under two working conditions are given based on the analysis of multiple experimental data. It is concluded that with regard to the surface texture density of the cylinder liner near the BDC of

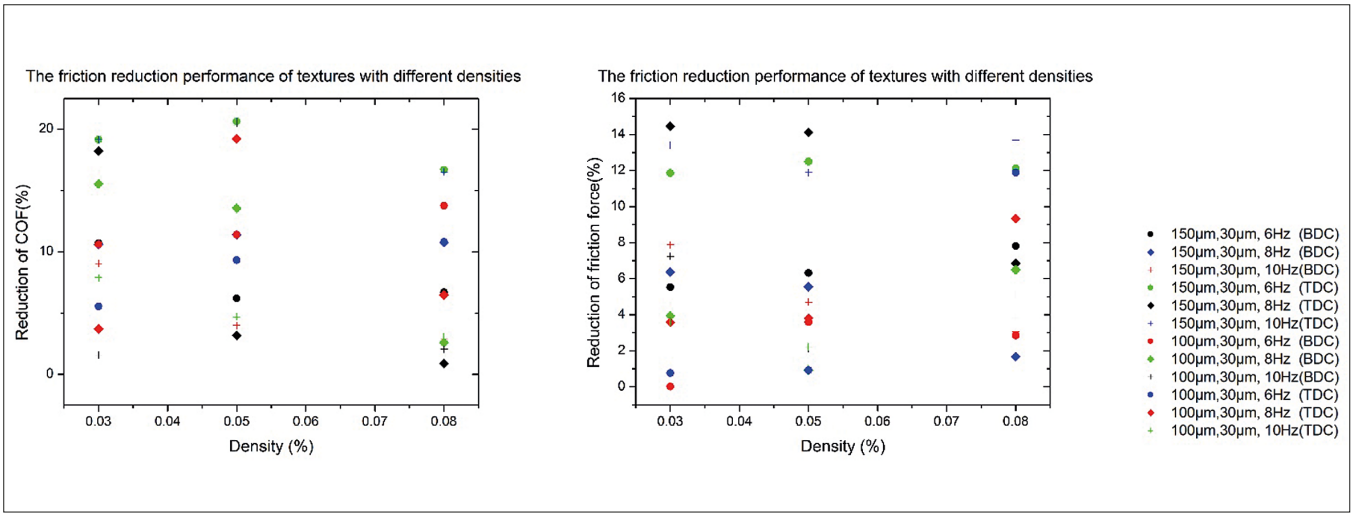

Fig. 26. The friction reduction performances of textures with different densities

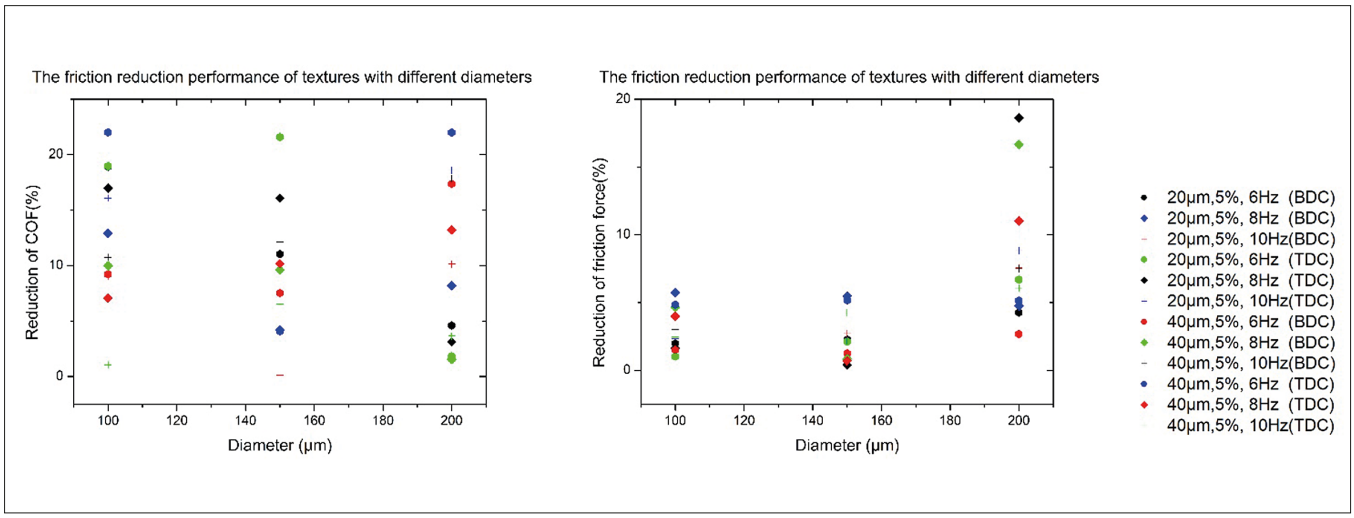

Fig. 27. The friction reduction performances of pits with different diameters

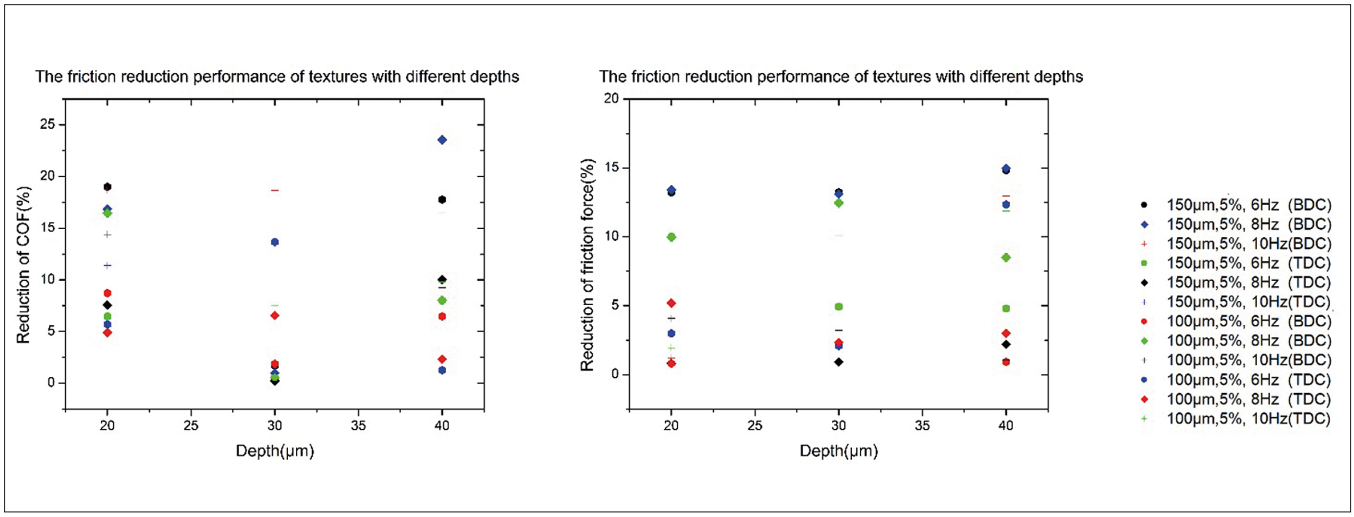

Fig. 28. The friction reduction performances of pits with different depths

the piston, more attention should be paid to the optimisation of pits diameter, whereas near the TDC of the piston, more attention should be paid to the optimisation of texture distribution density. Through the consideration of different parameters, the texture parameters of the upper, middle, and lower parts of the cylinder liner are reasonably configured to achieve the best friction reduction performance.

CONCLUSION

1. In the experiment, the conditions of low-speed oil starvation near the BDC and the conditions of high-temperature, high-pressure, and low-speed oil starvation near the TDC of an internal combustion engine were simulated. Comparing the average friction coefficient and friction force between the untextured surface and the surfaces with different textures, it was found that the textures with different parameters exhibited different degrees of anti-friction effect.
2. In the simulated BDC condition, the diameter parameter of the pits in the experiment had the greatest influence on the friction property of the surface, being able to reduce the friction coefficient by up to 24% and the friction force by 18%. The second was the pits depth parameter, which could reduce the friction coefficient by up to 17% and the friction force by up to 9%. The influence of the texture distribution density parameter on the friction property of the surface was minimal: the friction coefficient could be reduced by 11% at most and the friction force could be reduced by 7%.
3. In the simulated TDC condition, the distribution density parameter of the texture in the experiment had the greatest influence on the friction property of the surface, being able to reduce the friction coefficient by up to 19% and the friction force by 18%. The second most influential parameter was the pits depth, which could reduce the friction coefficient by up to 13% and the friction force by up to 12%. The influence of pits diameter on the friction property of the surface was minimal: the friction coefficient could be reduced by up to 10% and the friction force by up to 4%.
4. The friction pair of the cylinder liner and the piston ring are in different working and lubrication states at different

positions of the piston in an internal combustion engine. Therefore, textures with various design parameters can be arranged in different positions of the cylinder liner to achieve optimal friction performance. Based on the analysis of the experimental data, the design of the surface texture on the cylinder liner near the BDC should be paid more attention than the optimisation of the pits diameter, while the optimisation of texture distribution should be paid more attention during the design of the texture on the cylinder liner near the TDC.

REFERENCES

1. Lu X, Li Q, Zhang W, Guo Y, He T, Zou D. (2013) *Thermal analysis on piston of marine diesel engine*. Applied Thermal Engineering. 50:168–76.
2. Zabala B, Igartua A, Fernandez X, Priestner C, Ofner H, Knaus O, et al. (2017) *Friction and wear of a piston ring/cylinder liner at the top dead centre: Experimental study and modelling*. Tribology International. 106:23–33.
3. Gropper D, Wang L, Harvey TJ. (2016) *Hydrodynamic lubrication of textured surfaces: a review of modeling techniques and key findings*. Tribology International. 94:509–29.
4. Koura MM. (1980) *The effect of surface texture on friction mechanisms*. Wear. 63:1–12.
5. Kumar CP, Menezes PL, Kailas SV. (2008) *Role of surface texture on friction under boundary lubricated conditions*. Tribology Online. 3:12–8.
6. Li J, Xiong D, Dai J, Huang Z, Tyagi R. (2010) *Effect of surface laser texture on friction properties of nickel-based composite*. Tribology International. 43:1193–9.
7. Etsion I. (2004) *Improving tribological performance of mechanical components by laser surface texturing*. Tribology Letters. 17:733–7.
8. Arslan A, Masjuki HH, Varman M, Kalam MA, Quazi MM, Mahmud KAHA, et al. (2015) *Effects of texture diameter and depth on the tribological performance of DLC coating under lubricated sliding condition*. Applied Surface Science. 356:1135–49.
9. Wang X, Kato K, Adachi K. (2002) *The lubrication effect of micro-pits on parallel sliding faces of SiC in water*. Tribology Transactions. 45:294–301.
10. Wang X, Kato K, Adachi K, Aizawa K. (2003) *Loads carrying capacity map for the surface texture design of SiC thrust bearing sliding in water*. Tribology International. 36:189–97.
11. Ronen A, Etsion I, Kligerman Y. (2001) *Friction-reducing surface-texturing in reciprocating automotive components*. Tribology Transactions. 44:359–66.
12. Johansson S, Nilsson PH, Ohlsson R, Rosen B. (2011) *Experimental friction evaluation of cylinder liner/piston ring contact*. Wear. 271:625–33.
13. Caramia G, Carbone G, De Palma P. (2015) *Hydrodynamic lubrication of micro-textured surfaces: Two dimensional CFD-analysis*. Tribology International. 88:162–9.
14. Pettersson U, Jacobson S. (2003) *Influence of surface texture on boundary lubricated sliding contacts*. Tribology International. 36:857–64.
15. Ren N, Nanbu T, Yasuda Y, Zhu D, Wang Q. (2007) *Micro textures in concentrated-conformal-contact lubrication: effect of distribution patterns*. Tribology Letters. 28:275–85.
16. Syed I, Sarangi M. (2014) *Hydrodynamic lubrication with deterministic micro textures considering fluid inertia effect*. Tribology International. 69:30–8.
17. Menezes PL. (2016) *Surface texturing to control friction and wear for energy efficiency and sustainability*. The International Journal of Advanced Manufacturing Technology. 85:1385–94.
18. Tang W, Zhou Y, Zhu H, Yang H. (2013) *The effect of surface texturing on reducing the friction and wear of steel under lubricated sliding contact*. Applied Surface Science. 273:199–204.
19. Wakuda M, Yamauchi Y, Kanzaki S, Yasuda Y. (2003) *Effect of surface texturing on friction reduction between ceramic and steel materials under lubricated sliding contact*. Wear. 254:356–63.
20. Wroblewski E, Finke S. (2017) *Test bench measurement of friction loss in combustion engine*. Combustion Engines.
21. Etsion I, Burstein L. (1996) *A model for mechanical seals with regular microsurface structure*. Tribology Transactions. 39:677–83.
22. Dowson D, Taylor CM. (1979) *Cavitation in bearings*. Annual Review of Fluid Mechanics. 11:35–65.
23. Spikes HA. (1993) *Boundary lubrication and boundary films*. Tribology and Interface Engineering Series. 25:331–46.
24. Menezes PL, Kishore, Kailas SV. (2008) *Role of surface texture and roughness parameters in friction and transfer layer formation under dry and lubricated sliding conditions*. International Journal of Materials Research. 99:795–807.

25. Ma C, Gu W, Tu Q, Sun J, Bo Y. (2016) *Experimental investigation on frictional property of mechanical seals with varying dimple diameter along the radial face*. Advances in Mechanical Engineering. 8(8), 677-683.

26. Kurniawan R, Kiswanto G, Ko TJ. (2017) *Surface roughness of two-frequency elliptical vibration texturing (TFEVT) method for micro-dimple pattern process*. International Journal of Machine Tools & Manufacture. 116:77–95.

CONTACT WITH THE AUTHORS

Shen Wu
e-mail: wushen_smu@qq.com
Shanghai Maritime University
NO.1550 Haigang Av.Lingang New Cit
Pudong District, 201306 Shanghai
China

Pan Zhang
e-mail: panzhang@shmtu.edu.cn
Shanghai Maritime University
NO.1550 Haigang Av.Lingang New Cit
Pudong District, 201306 Shanghai
China

Haijun Wei
e-mail: hjwei@shmtu.edu.cn
Shanghai Maritime University
NO.1550 Haigang Av.Lingang New Cit
Pudong District, 201306 Shanghai
China

Lei Chen
e-mail: clinfo@126.co
Shanghai Maritime University
NO.1550 Haigang Av.Lingang New Cit
Pudong District, 201306 Shanghai
China